Orbital-free functional with sub-milliHartree errors for slabs

Pavel Okun
Department of Chemistry, University of California, Irvine, CA 92617, USA

Antonio C. Cancio
Department of Physics and Astronomy, Ball State University, Muncie, IN 47304, USA

Kieron Burke
Departments of Physics and Astronomy and of Chemistry, University of California, Irvine
(Dated: Monday 24th April, 2023)

Using principles of asymptotic analysis, we derive the exact leading correction to the Thomas-Fermi kinetic energy approximation for Kohn-Sham electrons for slabs. This asymptotic expansion approximation includes crucial quantum oscillations missed by standard semilocal density functionals. Because these account for the derivative discontinuity, chemical accuracy is achieved at fourth-order. The implications for both orbital-free electronic structure and exchange-correlation approximations are discussed.

Almost all modern density functional theory (DFT) calculations use the Kohn-Sham (KS) scheme [1], where only the exchange-correlation (XC) energy is approximated as a density functional [2]. Accuracy comes at the cost of solving self-consistently the KS equations for the orbitals. However, the KS kinetic energy, T_s, is also a density functional [2, 3]. If it could be approximated with sufficient accuracy, without incurring substantial additional computational cost, one would bypass the KS equations [4], speeding up every DFT calculation on the planet. The dream of orbital-free DFT lives on [5].

Thomas-Fermi (TF) theory [6, 7], the original DFT, is orbital-free, but is too crude for modern electronic structure calculations. First, T_s is typically far larger than the XC energy, so a far smaller fractional error is required. Second, via the Euler equation that follows from the variational principle [8], the functional derivative of T_s determines the density. In TF theory, the density errors dominate the energy error [9], while in KS calculations, the error in the self-consistent density is often negligible [10].

Over the decades, many attempts have been made to construct sufficiently accurate orbital-free approximations [4, 11–13], often aimed at a limited set of circumstances [14]. These include the original gradient expansion from slowly-varying densities [2, 15–17], generalizations of that expansion [14, 18], functionals designed for weakly interacting subsystems such as water molecules [19], and two-point functionals for use in materials calculations [20].

But Lieb and Simon showed long ago [21, 22] that, in a very specific semiclassical limit, TF theory becomes relatively exact. One approach to this Lieb-Simon (LS) limit is to take $\hbar \to 0$, keeping μ, the chemical potential, fixed. Expanding about this limit, potential functionals have been developed for the total energy of one-dimensional (1D) problems [23–26]. The dominant term is given by a TF calculation, but higher orders require subtle corrections to the gradient expansion, and depend on both the Maslov indices and whether the system is finite or extended. By resumming this asymptotic series for a linear half-well, the total energy of 10 non-interacting fermions was found to 33 digits [23].

Here, we demonstrate the capabilities of a potential functional to yield chemical accuracy [errors below 1 milliHartree (mH)] for a three-dimensional slab geometry, with a potential that varies in one direction but is uniform in the other two. We find excellent results when the leading correction is added to TF theory, and chemical accuracy when the next order is included, providing a systematic, parameter-free approach to orbital-free calculations.

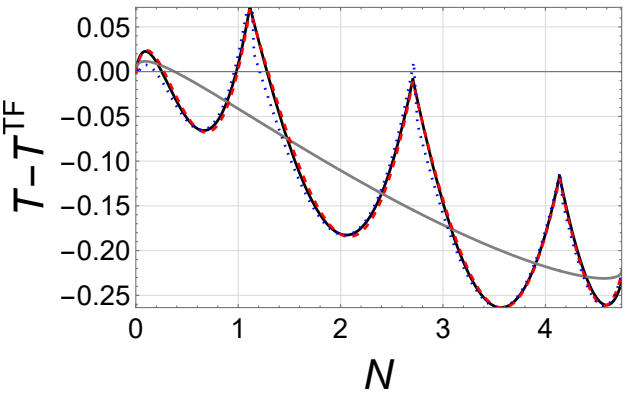

FIG. 1. Slab kinetic energy versus electron number (each per unit area) less its TF value (black), the second order gradient expansion approximation (gray), and its asymptotic expansion approximation (blue: crude, red: more accurate, see text). Cusps occur whenever a new band starts to be filled, i.e., derivative discontinuities.

Our calculation (a) shows how the asymptotic expansion corrects standard semi-local functionals to account for the derivative discontinuity [27, 28], (b) connects the rich field of semiclassical analysis of eigenvalue problems, including densities of states and the importance of Maslov indices [29, 30], to the construction of approximate functionals for non-trivial 3D problems, (c) explicitly connects the failures of semilocal functionals for stretched bonds (symmetry breaking) to the divergence of the asymptotic expansion [31], and (d) provides insight for creating functionals of chemical accuracy [32]. Figure 1 illustrates (a) showing

the deviation of the kinetic energy from its TF value, for a Pöschl-Teller (PT) slab with well depth 10. The standard density functional approximation, the gradient expansion (GEA), yields the smooth gray curve, which averages over the density of states. Our methodology accounts for the quantum oscillations characteristic of systems with discrete states, with errors almost too small to be visible here. It is unlikely any existing orbital-free appproximation can compete.

Background: Standard approaches to quantum mechanics yield functionals of the potential, such as approximate ground-state energies, $E[v]$. Via the celebrated Hohenberg-Kohn theorem [33], DFT uses functionals of the density, $\rho(\mathbf{r})$, instead. The semiclassical origin of any local density approximation begins, at least in one-dimensional cases, with the WKB approximation for individual eigenvalues [34]. A careful semiclassical expansion for the sum of the lowest eigenvalues yields expressions for the total energy of N (same-spin) fermions, occupying the lowest N levels, as a functional of the potential, $v(x)$ [25]. In 1D, this has been used to show the limitations of the gradient expansion [24], the starting point of many modern density functional approximations [35]. Moreover, asymptotic analysis shows that incredible accuracy is possible when many orders of the expansion are included [23].

However, almost all such previous work has been in 1D. While providing an excellent proof-of-principle, such 1D formulas cannot be directly applied to realistic electronic structure calculations. Here, we apply this technology to a three-dimensional problem, namely a slab with a potential profile $v(x)$, but uniform in the other two directions. While somewhat artificial, this geometry allows comparison with any existing orbital-free density functional [18]. By choosing a $v(x)$ that is the sum of two potential wells (a dimer), separated by a distance R, we mimic certain aspects of more realistic calculations, such as binding energies as a function of bond lengths in diatomics [36].

Theory: Consider a 1D well $v(x)$, but uniform in the other two directions (which have length $L \to \infty$ and periodic boundary conditions). The eigenstates are two-dimensional free electron bands, with energies $\epsilon_j(K) = \epsilon_j + K^2/2$, where ϵ_j is the j-th eigenvalue in the 1D well, and K is the parallel wavevector (see Fig. S1 in the supplementary information). Summing over parallel directions in the continuum limit, assuming double occupation, yields

$$N(\mu) = \sum_{j=0}^{\infty} \frac{(\mu-\epsilon_j)_+}{\pi}, \qquad E(\mu) = \sum_{j=0}^{\infty} \frac{(\mu^2-\epsilon_j^2)_+}{2\pi}, \quad (1)$$

where N and E are the particle number and energy per unit area, respectively, and $x_+ = x$ for $x > 0$, and 0 otherwise. The density of states, $\mathrm{d}N/d\mu$, consists of constants (2D uniform gas), with steps up at each ϵ_j (Fig. S4). We use atomic units ($\hbar = m_e = 1$), so energies are in Hartrees and distances are in Bohr radii. We populate our slabs with non-interacting KS electrons.

Semiclassical expansion of the eigenvalues yields [37]

$$s^{(0)}(\epsilon_j) + \Delta s^{(2)}(\epsilon_j) + \Delta s^{(4)}(\epsilon_j) + \cdots = j + \frac{1}{2}, \quad (2)$$

where $j = 0, 1, \cdots$, labels the levels and $1/2$ is the Maslov index with two turning points. Here, $s^{(0)}(\epsilon)$ is the classical action per unit of phase space, $\int dx\, p(\epsilon,x)/\pi$, where $p(\epsilon,x) = \sqrt{2[\epsilon - v(x)]}$ is the momentum, and all x integrals are understood to run only between classical turning points. The first term is from WKB, while higher orders involve higher derivatives of the potential. Using just the first term, March and Plaskett [38] showed that, in the semiclassical limit, non-interacting TF theory could be derived (as a potential or a density functional) by summing the lowest N energy levels, both for 1D and radial 3D problems. Recently [23–26, 39], this procedure was generalized using the Euler-Maclaurin summation formula, to yield the corresponding series for the sum of the lowest N eigenvalues, order by order, but only for 1D.

We expand $N(\mu)$ and $E(\mu)$ order by order for a slab with a symmetric single-well potential:

$$\begin{aligned} N(\mu) &= N^{\mathrm{TF}}(\mu) + \Delta N^{(2s)}(\mu) + \Delta N^{(2o)}(\mu), \\ E(\mu) &= E^{\mathrm{TF}}(\mu) + \Delta E^{(2s)}(\mu) + \Delta E^{(2o)}(\mu), \end{aligned} \quad (3)$$

where s denotes a smooth correction, o an oscillating one. Inversion, order-by-order, of $N(\mu)$ yields

$$\mu(N) = \mu^{\mathrm{TF}}(N) + \Delta\mu^{(2s)}(N) + \Delta\mu^{(2o)}(N), \quad (4)$$

which can be inserted, order-by-order, into $E(\mu)$ to generate the expansion of $E(N)$, and likewise for $T(N)$. Asymptotic expansion approximation (AEA) denotes application of these expressions to a finite system. If the oscillatory terms are neglected, AEA reduces to GEA. Such terms are indeed zero for a slowly-varying electron gas, where $\mu > v(x)$ everywhere and there are no classical turning points. But they occur and are important for all atoms and molecules and solids with μ below the KS potential.

Using the Euler-Maclaurin formula to approximate sums, yields the familiar TF theory to lowest order:

$$N^{\mathrm{TF}} = \int \frac{dx}{3\pi^2}\, p_{\mathrm{F}}^3, \; E^{\mathrm{TF}} = \int \frac{dx}{3\pi^2} \left[\frac{3}{10}p_{\mathrm{F}}^2 + v(x)\right] p_{\mathrm{F}}^3, \quad (5)$$

where $p_{\mathrm{F}}(x) = p(\mu,x)$. The first term in the energy is the kinetic contribution. The familiar results of (non-interacting) TF DFT in 3D for spin-unpolarized systems are recovered using $\rho(x) = \delta E/\delta v(x)$ for fixed N, yielding $\rho^{\mathrm{TF}}(x) = p_{\mathrm{F}}(x)^3/(3\pi^2)$, and isolating $T^{\mathrm{TF}}[\rho]$. Solution of the Euler equation then yields identical results to those of the potential functional.

A principal achievement of this work is the derivation of the next terms in the semiclassical expansion. Earlier summation techniques [23–25] become considerably more involved, due to the extra integration over continuum states in the perpendicular directions. The smooth corrections are

$$\Delta N^{(2s)} = -\frac{1}{3\pi}\frac{dI}{d\mu}, \qquad \Delta E^{(2s)} = \mu\,\Delta N^{(2s)} - 2\Delta T^{(2s)}, \quad (6)$$

				Errors (mH)								
				Potential Functionals					Density Functionals			
M	D	N	T/N	TF	GEA2	AEA2'	AEA2	AEA4'	TF	GEA2	MGE2	GEA4
1	12.685	1.293	3.059	−87	−126	−29	−2.74	0.0889	−156	−41	−8	−2
2	36.000	6.525	8.728	−85	−125	−14	−0.92	0.0223	−159	−35	1	−6
3	70.971	18.318	17.233	−85	−125	−9	−0.46	0.0087	−162	−31	7	−7
4	117.599	39.293	28.573	−84	−125	−7	−0.28	0.0042	−164	−28	11	−6
5	175.883	72.075	42.748	−84	−125	−6	−0.18	0.0024	−165	−26	14	−6
6	245.824	119.288	59.757	−84	−125	−5	−0.13	0.0015	−166	−25	16	−6
7	327.422	183.555	79.602	−84	−125	−4	−0.10	0.0010	−167	−24	18	−6
8	420.677	267.500	102.281	−84	−125	−3	−0.08	0.0007	−168	−23	19	−6
9	525.589	373.746	127.795	−84	−125	−3	−0.06	0.0005	−168	−22	21	−5
10	642.157	504.918	156.145	−84	−125	−3	−0.05	0.0004	−169	−21	22	−5

TABLE I. Kinetic energy per particle for Pöschl-Teller slabs with $D = 2\epsilon_M$ and $\mu = D/2$. Here G(A)EAp is the p-th order gradient (asymptotic) expansion approximation, while MGE2 is a generalized gradient approximation (GGA) [18]. The rightmost columns are density functionals evaluated on the exact density.

where $\Delta T^{(2s)} = -I/(6\pi)$ and $I = \int dx\, v''(x) p_{\rm F}(x)/(8\pi)$. The oscillating corrections are

$$\Delta N^{(2o)} = \frac{q}{2\tau}, \quad \Delta E^{(2o)} = \frac{\mu q}{2\tau}, \quad \Delta T^{(2o)} = \frac{\pi s^{(0)} q}{4\tau^2}, \quad (7)$$

where $\tau = \pi s^{(0)\prime}(\mu) = \int dx/p_{\rm F}(x)$ is the classical time to cross the well at energy μ, while $q = 1/12 - \langle s \rangle^2$ oscillates between energy levels, i.e., contains the quantum oscillations, and is entirely missed by the gradient expansion. Here, $\langle x \rangle = x - \lfloor x + 1/2 \rfloor$ so q oscillates between 1/12 and -1/6. These expressions are quite general, and apply to *any* $v(x)$ with two turning points. These analytic results can be favorably contrasted with the numerical fitting of Ref. [40] for the leading corrections to LDA exchange. We define two AE approximations: AEA2' uses $s^{(0)}$ in q, $[q = 1/12 - \langle s^{(0)} \rangle^2]$, while AEA2 uses $s^{(2)}$ (see appendix C in the supplemental information). Both capture the leading asymptotic corrections to TF, but the latter is more accurate away from the limit. As we illustrate below, these are the exact asymptotic corrections to TF theory for such problems. We believe this is the first time such a term has been analytically derived for a functional in 3D.

Pöschl-Teller slabs: Our next step is to apply these formulas to a specific problem. Our prototypical well is the Pöschl–Teller well, with $v(x) = D \tanh^2 x$. Such potentials have been used in semiconductor physics [41, 42], and are chosen here for ease of computation. The TF PT particle number and total energy are

$$\frac{N^{\rm TF}}{\sqrt{2D^3}} = \frac{c^2(3-2c)}{3\pi}, \qquad \frac{E^{\rm TF}}{\sqrt{2D^5}} = \frac{c^3}{3\pi}\left(4 - \frac{9c}{2} + \frac{6c^2}{5}\right), \quad (8)$$

where $c = 1 - \sqrt{1-\mu/D}$, and $T^{\rm TF} = 3(\mu N^{\rm TF} - E^{\rm TF})/2$. The second order contributions are

$$\begin{aligned}
\Delta N^{(2)} &= \sqrt{2D}[c\,(4-3c) - 24\,\langle s \rangle^2\,(1-c)]/(48\pi), \\
\Delta E^{(2)} &= \mu[\Delta N^{(2)} + \sqrt{2D}(4 - 6c + 3c^2)/(96\pi)], \\
\Delta T^{(2)} &= -\sqrt{2D^3}[c^2(4-3c) + 96\,\langle s \rangle^2\,(1-c)^2]c/(192\pi),
\end{aligned} \quad (9)$$

where $\Delta N^{(2)} = \Delta N^{(2s)} + \Delta N^{(2o)}$. Here $s^{(0)} = \sqrt{2D}c$ and $\Delta s^{(2)} = 1/(8\sqrt{2D})$.

Numerical results: We insert exact eigenvalues and eigenfunctions for the PT slab [43], and evaluate energies and particle numbers. We approach the LS limit by deepening the well while keeping μ/D fixed (at 1/2), which is a slightly different approach to taking $\hbar \to 0$ and scaling the particle number [44], and explains why the normalization is almost (but not quite) fixed in the scaled densities of Fig. S6. We set $D = 2\epsilon_M$, so μ is just below the appearance of a new level. Table I reports many approximations to the kinetic energy for this sequence of ever deeper wells. Here T/N is the exact kinetic energy per particle in Hartrees, but errors are in milliHartrees. The next set of columns are errors of approximate potential functionals calculated to that order for the exact particle number N, i.e., finding the approximate μ that yields the correct N. The first column is the error in the TF prediction, which starts out of order 3%, and shrinks to less than 0.1%, consistent with the LS theorem [21, 22]. TF is particularly good for our slab, due to the smoothness of the density in the x-direction and uniformity in the other two (see Fig. S6). The (2nd-order) gradient expansion (GEA2) worsens the result, but AEA2 has much smaller errors, especially for larger D. In fact, errors are less than a mH for all but the shallowest well. The 4-th order AEA has errors below 0.1 mH for all wells, reaching μH accuracy for the deepest ones. This was calculated numerically, as described in appendix C. This illustrates how just a few terms in the asymptotic expansion can yield chemical accuracy for non-interacting kinetic energies.

The right-hand set of columns are density functionals evaluated on the exact density. Unusually, TF does better self-consistently than on the exact density [10, 45], but GEA2 is improved. The MGE2 (gradient expansion with coefficient modified to recover asymptotics of atoms) is better for small wells, but comparable in the asymptotic limit. The fourth-order GEA is better, but not nearly as good as AEA2.

This table only tests one value of μ/D, but similar trends hold for any value. In Fig. 2, we plot errors for a shallow PT slab, $D = 3$, as a function of N, far from the LS limit. Our 2nd order approximation is typically better than GEA2 and

			Errors (mH)			
			IP		μ	
M	IP	μ	TF	AEA2	TF	AEA2
1	5.557	6.342	−63	−3	−242	0.010
2	17.607	18.000	−172	−131	−239	0.013
3	35.224	35.486	−204	−166	−238	0.009
4	58.603	58.799	−217	−180	−237	0.006
5	87.784	87.941	−224	−187	−237	0.004
6	122.781	122.912	−227	−191	−237	0.003
7	163.599	163.711	−230	−194	−237	0.003
8	210.240	210.339	−231	−196	−237	0.002
9	262.707	262.794	−232	−197	−237	0.002
10	321.000	321.079	−233	−198	−237	0.001

TABLE II. The ionization potential (double the energy needed to lower N by 1/2) and the chemical potential for the slabs of Table I. Table S1 shows more approximations to these quantities.

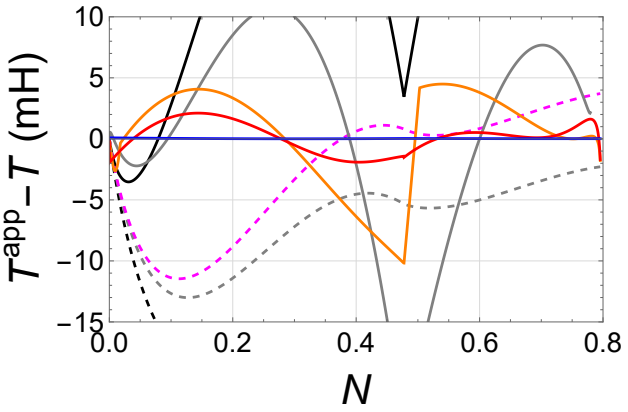

FIG. 2. Kinetic energy errors for a shallow PT slab ($D = 3$) for various N. Legend: TF (black), GEA2 (gray), MGE2 (magenta), AEA2' (orange), AEA2 (red), AEA4' (blue). Dashed lines denote density functionals acting on the exact density.

even MGE2 in this range, and all are beaten by inclusion of the next order. Both this figure and Fig. 1 show that AEA2 includes cusps in the kinetic energy as a function of N, the infamous derivative discontinuity that is the source of many errors in modern DFT calculations [27, 28]. The resemblance with Fig. 9 of Ref. [46] (non-interacting electrons in a Coulomb potential) is striking. But that work was for a specific potential, whereas our expressions are potential functionals.

Energy differences: While it is important to demonstrate the validity of our expressions on total energies, essentially all useful DFT calculations are of energy differences, such as ionization potentials and binding energies of molecules (infinitesimal differences determine bond lengths and lattice parameters). The asymptotic behavior of ionization potentials of neutral atoms was studied in Ref. [47], where Dirac exchange (i.e., its local density approximation) in a KS calculation was found to match the exact result (Hartree-Fock), even capturing variations across a row of the (very extended) non-relativistic periodic table. Moreover, the average over such a row matched that of extended interacting TF theory. We know of no results finding corrections to the LS limit for binding energies.

In Table II we calculate electron removal energies in two distinct ways. To simulate an ionization potential (IP) of a molecule, we remove 0.5 electrons per unit area, since removal of a single electron is just given by μ (the true IP of a metal). In the case closest to the limit ($M = 10$) this removes just 0.1% of the particle number. The left-hand errors are those found from total energy differences, in which AEA2 is surprisingly poor. This is because the total energy itself is a smooth function of N (see Figs. S9 and S10) and AEA2 for $E(N)$ has no oscillations (the cusps in Fig. 1 are in the kinetic energy, which does). On the other hand, $\mu^{\rm AEA2}(N)$ does contain quantum oscillations, as shown in Fig. S11. The right-hand side of the table shows much better results from μ in AEA2. This illustrates the subtleties of taking derivatives of the oscillating terms, which are typically one order larger than those of the corresponding smooth terms. The origin of this phenomena can be seen by considering the function Cx for $x >> 1$. Clearly $Cx >> C\langle x\rangle$, but their derivatives are of comparable magnitude.

Our last test is the most stringent. We consider the sum of two identical PT slabs (the PT dimer) as a function of their separation, R, as a mimic of the calculation of the binding energy of a molecule. At $R = 0$, this is a single PT slab of depth $2D$, where D is the depth of each individual PT slab. Up to $R_c = 2\,\text{asech}\sqrt{2/3} = 1.31696$, there is a single minimum, but beyond R_c there is a double well (see Fig. S8). We perform our calculation only for R up to R_c, as the nature of the asymptotic expansion changes in the double well regime. We keep N fixed throughout. Table III shows the result. For $R < R_c/2$, our results for energy differences are similar to those for total energies, with AEA4' yielding chemical accuracy. However, as $R \to R_c$, the AEA4' error grows vastly. This is because there are turning points in the complex plane yielding sub-dominant contributions. Usually these are tiny, but they become comparable to (and overwhelm) those of the real turning points, eventually switching the asymptotic series to that of two isolated PT slabs. This is analogous to the Coulson-Fischer point as bonds are stretched for XC [48]. Here, we can clearly identify this difficulty with the asymptotic nature of the expansion. In fact, optimal truncation [39] dictates replacing AEA4' with AEA2 at about $R = 0.8R_c$, thereby avoiding the divergence. The failure in AEA4' is due to the failure of WKB which we show in Table S6, as our numerical evaluation of AEA4' uses the semiclassical eigenvalues (see appendix C). Moreover the failure in WKB affects the AEA4' energy through the AEA4' chemical potential. When evaluated on the exact μ, AEA4' yields chemical accuracy (almost) everywhere.

Conclusions: The results shown here bring the proof-of-principle from earlier 1D studies a significant step closer to algorithms that might be employed for realistic orbital-free electronic structure calculations. We have compared the leading terms in the semiclassical expansion with modern

		Errors (mH)									
		Potential Functionals					Exact Density or μ				
R/R_c	$T-2T_A$	TF	GEA2	AEA2'	AEA2	AEA4'	TF	GEA2	MGE2	GEA4	AEA4'(μ)
0	0.792	27	29	32	6.1	−0.04	−23.8	−10.8	−7.1	−12	−0.23
0.1	0.783	29	31	33	6.9	−0.04	−23.0	−10.8	−7.2	−12	−0.24
0.2	0.759	32	36	33	7.1	−0.03	−20.5	−10.2	−7.3	−12	−0.24
0.25	0.742	34	39	32	7.1	−0.02	−18.8	−9.9	−7.3	−12	−0.25
0.3	0.722	35	42	32	7.1	0.01	−16.7	−9.4	−7.2	−12	−0.25
0.4	0.672	39	49	31	6.8	0.12	−11.8	−8.1	−7.1	−12	−0.25
0.5	0.613	42	56	29	6.0	0.51	−6.0	−6.4	−6.6	−11	−0.22
0.6	0.546	43	61	27	5.5	1.95	0.3	−4.5	−5.9	−9	−0.08
0.7	0.476	43	65	25	4.6	7.82	6.5	−2.4	−5.0	−8	0.27
0.75	0.441	42	65	24	4.1	16.49	9.5	−1.3	−4.5	−7	0.57
0.8	0.406	40	65	22	3.4	37.23	12.3	−0.3	−3.9	−6	0.95
0.9	0.337	36	63	20	2.7	315.82	17.3	1.6	−3.0	−4	2.00
1	0.271	30	60	19	2.3	−37.33	21.3	3.1	−2.2	−3	−0.69

TABLE III. The kinetic binding energies, $T-2T_A$, for a series of PT dimers made from 2, $D=3$, PT slabs. T is the exact kinetic energy and T_A is the kinetic energy of an isolated $D=3$ PT slab. The occupation in each well is fixed at $N=3/\pi$. AEA4'(μ) is the fourth order AEA evaluated on the exact chemical potential. All other approximations are defined as in Table I. We increase the separation between the PT centers to model bond breaking. The depth of each dimer is given by $\mathcal{D}=6\,\mathrm{sech}^2(R/2)$.

orbital-free density functionals, and shown how they achieve much greater accuracy. Our potential functionals capture the derivative discontinuities to which many of the failures of modern density functionals are attributed. Moreover, we have shown how inclusion of these step-like features generates quantum oscillations which reduce errors by orders of magnitude over smooth approximations such as GGAs.

Does our potential functional work only for slabs? In fact, it could be applied to any geometry at all, by simply designating the direction of the gradient of the potential as the local x-direction, and calculating a contribution to the energy density at that point. Choices would need to be made about effective Maslov indices, etc., so some experimentation would be required. Such an application almost certainly would not yield the exact semiclassical expansion for an arbitrary geometry, but it might generate an excellent approximation to it. After all, it is guaranteed to be asymptotically exact for slabs. A simple test of this concept would be spherical systems, i.e., atoms and ions, where the asymptotic behavior of both $T_{\rm S}$ and the XC energy has been well studied [32, 40, 46, 48–50].

Is it a problem that our functional is a potential functional, and not a density functional? In principle, it is not, as the ground-state density can be extracted from a total energy approximation by taking the functional derivative with respect to the potential at fixed N. Then the Lieb construction can be applied to create a density functional from a potential functional [51, 52]. For a local density approximation to T_s, it makes no difference whether you choose to write it as a potential or a density functional, as the resulting Euler equations are identical for either choice. But for the GEA and the corrections discussed here, it does, and we have no a priori way to know which form might be more accurate (in general, densities are smoother than potentials, and these $\hbar$ expansions are asymptotic, which may make density functionals more accurate).

Could these techniques be applied to the XC energy? Yes, but there is an important difficulty. Consider exchange. Our most accurate results are currently obtained by fitting highly accurate atomic data for atoms up to $Z=100$, because we do not have the analytic results given here [40]. The technology for generating asymptotic expansions for sums must be generalized to do the double sum in the exchange energy, but one also needs the semiclassical expansion for the KS density matrix with real turning points [53]. Reference [23] gives us a glimpse of the nirvana that might be achieved if we could overcome that one difficulty.

We thank the NSF (CHE-2154371) for funding. A longer paper including details of the derivations, exact results for PT slabs, and limiting cases, is in preparation.

[1] W. Kohn and L. J. Sham, Self-consistent equations including exchange and correlation effects, Phys. Rev. **140**, A1133 (1965).
[2] R. M. Dreizler and E. K. Gross, *Density Functional Theory: An Approach to the Quantum Many-Body Problem*, 1st ed. (Springer-Verlag Berlin Heidelberg, Berlin Heidelberg, 1990).
[3] R. G. Parr and W. Yang, *Density-Functional Theory of Atoms and Molecules (International Series of Monographs on Chemistry)* (Oxford University Press, USA, 1994).
[4] V. L. Lignères and E. A. Carter, An introduction to orbital-free density functional theory, in *Handbook of Materials Modeling: Methods*, edited by S. Yip (Springer Netherlands, Dordrecht, 2005) pp. 137–148.
[5] W. Mi, K. Luo, S. B. Trickey, and M. Pavanello, Orbital-free density functional theory: An attractive electronic structure

method for large-scale first-principles simulations, In prep (2023).
[6] L. H. Thomas, The calculation of atomic fields, Mathematical Proceedings of the Cambridge Philosophical Society **23**, 542–548 (1927).
[7] E. Fermi, Rend. Acc. Naz. Lincei **6** (1927).
[8] E. H. Lieb, Density functionals for coulomb systems, International Journal of Quantum Chemistry **24**, 243 (1983), https://onlinelibrary.wiley.com/doi/pdf/10.1002/qua.560240302.
[9] M.-C. Kim, E. Sim, and K. Burke, Understanding and reducing errors in density functional calculations, Phys. Rev. Lett. **111**, 073003 (2013).
[10] E. Sim, S. Song, S. Vuckovic, and K. Burke, Improving results by improving densities: Density-corrected density functional theory, Journal of the American Chemical Society **144**, 6625 (2022), pMID: 35380807.
[11] E. Fabiano, F. Sarcinella, L. A. Constantin, and F. Della Sala, Kinetic energy density functionals based on a generalized screened coulomb potential: Linear response and future perspectives, Computation **10**, 10.3390/computation10020030 (2022).
[12] T. A. Wesolowski and Y. A. Wang, *Recent Progress in Orbital-free Density Functional Theory* (World Scientific, 2013).
[13] W. C. Witt, B. G. del Rio, J. M. Dieterich, and E. A. Carter, Orbital-free density functional theory for materials research, Journal of Materials Research **33**, 777 (2018).
[14] K. Luo, V. V. Karasiev, and S. B. Trickey, A simple generalized gradient approximation for the noninteracting kinetic energy density functional, Phys. Rev. B **98**, 041111 (2018).
[15] D. Kirzhnits, Quantum corrections to the thomas-fermi equation, Sov. Phys. JETP **5**, 64 (1957).
[16] L. Šamaj and J. K. Percus, Recursion representation of gradient expansion for free fermion ground state in one dimension, The Journal of Chemical Physics **111**, 1809 (1999).
[17] W. Yang, Gradient correction in thomas-fermi theory, Phys. Rev. A **34**, 4575 (1986).
[18] L. A. Constantin, E. Fabiano, S. Laricchia, and F. Della Sala, Semiclassical neutral atom as a reference system in density functional theory, Phys. Rev. Lett. **106**, 186406 (2011).
[19] J. M. G. Lastra, J. W. Kaminski, and T. A. Wesolowski, Orbital-free effective embedding potential at nuclear cusps, The Journal of Chemical Physics **129**, 074107 (2008).
[20] Y. A. Wang, N. Govind, and E. A. Carter, Orbital-free kinetic-energy density functionals with a density-dependent kernel, Phys. Rev. B **60**, 16350 (1999).
[21] E. H. Lieb and B. Simon, Thomas-fermi theory revisited, Phys. Rev. Lett. **31**, 681 (1973).
[22] E. H. Lieb and B. Simon, The thomas-fermi theory of atoms, molecules and solids, Advances in Mathematics **23**, 22 (1977).
[23] M. V. Berry and K. Burke, Exact and approximate energy sums in potential wells, Journal of Physics A: Mathematical and Theoretical **53**, 095203 (2020).
[24] K. Burke, Leading correction to the local density approximation of the kinetic energy in one dimension, The Journal of Chemical Physics **152**, 081102 (2020).
[25] K. Burke, Deriving approximate density functionals with asymptotics, Faraday Discuss. 10.1039/D0FD00057D (2020).
[26] P. Okun and K. Burke, Semiclassics: The hidden theory behind the success of dft, in *Density Functionals for Many-Particle Systems: Mathematical Theory and Physical Applications of Effective Equations*, edited by B.-G. Englert, M.-I. Trappe, and H. Siedentop (World Scientific Publishing Company, Singapore, 2023) pp. 179–249.
[27] P. Mori-Sánchez, A. J. Cohen, and W. Yang, Localization and delocalization errors in density functional theory and implications for band-gap prediction, Phys. Rev. Lett. **100**, 146401 (2008).
[28] L. Kronik and S. Kümmel, Piecewise linearity, freedom from self-interaction, and a coulomb asymptotic potential: three related yet inequivalent properties of the exact density functional, Phys. Chem. Chem. Phys. **22**, 16467 (2020).
[29] M. Brack and R. Bhaduri, *Semiclassical Physics*, 1st ed. (Routledge, Boca Raton, 2003).
[30] M. C. Gutzwiller, *Chaos in Classical and Quantum Mechanics* (Springer, New York, NY, 1990).
[31] A. J. Cohen, P. Mori-Sánchez, and W. Yang, Insights into current limitations of density functional theory, Science **321**, 792 (2008).
[32] A. Cancio, G. P. Chen, B. T. Krull, and K. Burke, Fitting a round peg into a round hole: Asymptotically correcting the generalized gradient approximation for correlation, The Journal of Chemical Physics **149**, 084116 (2018).
[33] P. Hohenberg and W. Kohn, Inhomogeneous electron gas, Phys. Rev. **136**, B864 (1964).
[34] A. Ruzsinszky, J. P. Perdew, and G. I. Csonka, Binding energy curves from nonempirical density functionals ii. van der waals bonds in rare-gas and alkaline-earth diatomics, The Journal of Physical Chemistry A **109**, 11015 (2005).
[35] J. P. Perdew, K. Burke, and M. Ernzerhof, Generalized gradient approximation made simple, Phys. Rev. Lett. **77**, 3865 (1996).
[36] J. P. Perdew, A. Savin, and K. Burke, Escaping the symmetry dilemma through a pair-density interpretation of spin-density functional theory, Phys. Rev. A **51**, 4531 (1995).
[37] C. M. Bender and S. A. Orszag, *Advanced Mathematical Methods for Scientists and Engineers I: Asymptotic Methods and Perturbation Theory* (Springer, Verlag New York, 1999).
[38] N. H. March and J. S. Plaskett, The relation between the wentzel-kramers-brillouin and the thomas-fermi approximations, Proceedings of the Royal Society of London. Series A. Mathematical and Physical Sciences **235**, 419 (1956), http://rspa.royalsocietypublishing.org/content/235/1202/419.full.pdf+h
[39] P. Okun and K. Burke, Asymptotics of eigenvalue sums when some turning points are complex, Journal of Physics A: Mathematical and Theoretical **55**, 394003 (2022).
[40] N. Argaman, J. Redd, A. C. Cancio, and K. Burke, Leading correction to the local density approximation for exchange in large-z atoms, Phys. Rev. Lett. **129**, 153001 (2022).
[41] J. Radovanović, V. Milanović, Z. Ikonić, and D. Indjin, Intersubband absorption in pöschl–teller-like semiconductor quantum wells, Physics Letters A **269**, 179 (2000).
[42] R. R. Hartmann and M. E. Portnoi, Two-dimensional dirac particles in a pöschl-teller waveguide, Scientific Reports **7**, 11599 (2017).
[43] M. M. Nieto, Exact wave-function normalization constants for the $B_0 tanh z - U_0 cosh^{-2} z$ and pöschl-teller potentials, Phys. Rev. A **17**, 1273 (1978).
[44] A. Cangi, D. Lee, P. Elliott, and K. Burke, Leading corrections to local approximations, Phys. Rev. B **81**, 235128 (2010).
[45] S. Vuckovic, S. Song, J. Kozlowski, E. Sim, and K. Burke, Density functional analysis: The theory of density-corrected dft, Journal of Chemical Theory and Computation **15**, 6636

(2019).
[46] K. Burke, A. Cancio, T. Gould, and S. Pittalis, Locality of correlation in density functional theory, The Journal of Chemical Physics **145**, 054112 (2016).
[47] L. A. Constantin, J. C. Snyder, J. P. Perdew, and K. Burke, Communication: Ionization potentials in the limit of large atomic number, The Journal of Chemical Physics **133**, 241103 (2010).
[48] A. D. Kaplan, B. Santra, P. Bhattarai, K. Wagle, S. T. u. R. Chowdhury, P. Bhetwal, J. Yu, H. Tang, K. Burke, M. Levy, and J. P. Perdew, Simple hydrogenic estimates for the exchange and correlation energies of atoms and atomic ions, with implications for density functional theory, The Journal of Chemical Physics **153**, 074114 (2020).
[49] P. Elliott and K. Burke, Non-empirical derivation of the parameter in the b88 exchange functional, Canadian Journal of Chemistry **87**, 1485 (2009).
[50] H. Kunz and R. Rueedi, Atoms and quantum dots with a large number of electrons: The ground-state energy, Phys. Rev. A **81**, 032122 (2010).
[51] A. Cangi, D. Lee, P. Elliott, K. Burke, and E. K. U. Gross, Electronic structure via potential functional approximations, Phys. Rev. Lett. **106**, 236404 (2011).
[52] A. Cangi, E. K. U. Gross, and K. Burke, Potential functionals versus density functionals, Phys. Rev. A **88**, 062505 (2013).
[53] P. Elliott, A. Cangi, S. Pittalis, E. K. U. Gross, and K. Burke, Almost exact exchange at almost no computational cost in electronic structure, Phys. Rev. A **92**, 022513 (2015).
[54] F. Sagredo and K. Burke, Confirmation of the pplb derivative discontinuity: Exact chemical potential at finite temperatures of a model system, Journal of Chemical Theory and Computation **16**, 7225 (2020).
[55] D. J. Griffiths, *Introduction to quantum mechanics* (Pearson Prentice Hall, 2005).
[56] E. H. Lieb, The stability of matter, Rev. Mod. Phys. **48**, 553 (1976).

Appendix A: Bands and density of states for PT slabs

This section contains plots of the bands and density of states (DOS) for a (single) Pöschl-Teller (PT) slab. It relates the qualitative behavior of the kinetic energy to the behavior of the DOS within various AE approximations.

Figure S1 shows the simple shape of the PT slab bands, which are free-electron like in the two directions perpendicular to $v(x)$ and begin at each of the eigenvalues of the 1D well. The system is a band metal.

Figure S2 shows the number staircase (integrated DOS) for a given PT slab. The function is rather smooth, making it difficult to see differences between approximations. However, there are kinks in the exact curve whenever a new band begins to be occupied. Both the TF and GEA2 curves have no such kinks. Although TF is often considered to give 'the' smooth curve, there is a small but finite correction from the second order GEA.

Figure S3 plots the errors (defined as approximate minus exact) in the number staircase of the various approximations. The TF and GEA2 error curves have kinks because they are smooth, but the exact curve is not. The orange curve is AEA2', which only accounts for the leading behavior of the phase, while the red curve is AEA2, which includes the next contribution to the phase. Their differ-

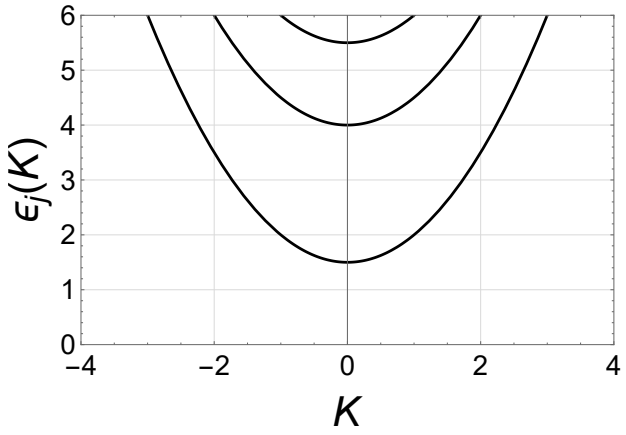

FIG. S1. The eigenvalues of the, $D = 6$, PT slab as a function of the parallel wave vector K.

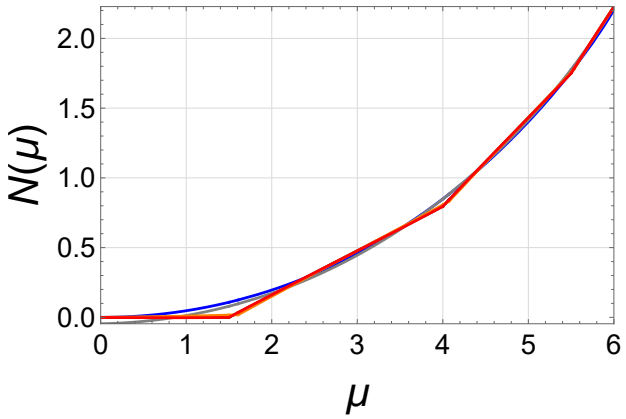

FIG. S2. The, $D = 6$, PT slab occupation (black), and its TF (blue), GEA2 (gray), AEA2' (orange), and AEA2 (red) approximations.

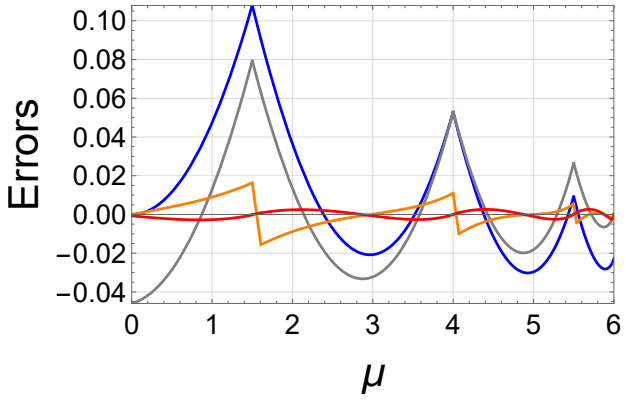

FIG. S3. The errors in Fig. S2.

ence becomes negligible for sufficiently large μ (both are asymptotically correct), but AEA2 clearly has smaller errors for small μ.

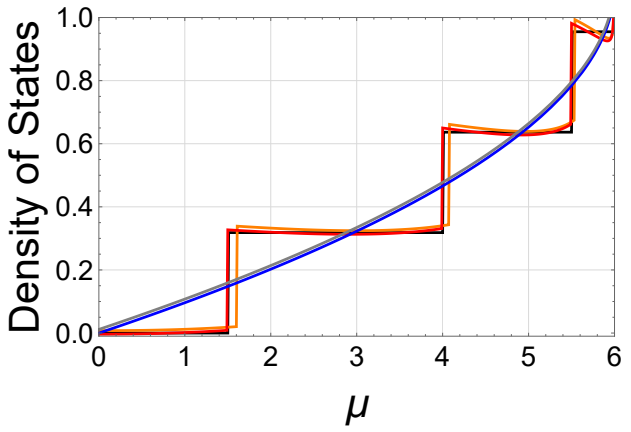

FIG. S4. The, $D = 6$, PT slab density of states $dN/d\mu$ (black), and its TF (blue), GEA2 (gray), AEA2' (orange), and AEA2 (red) approximations.

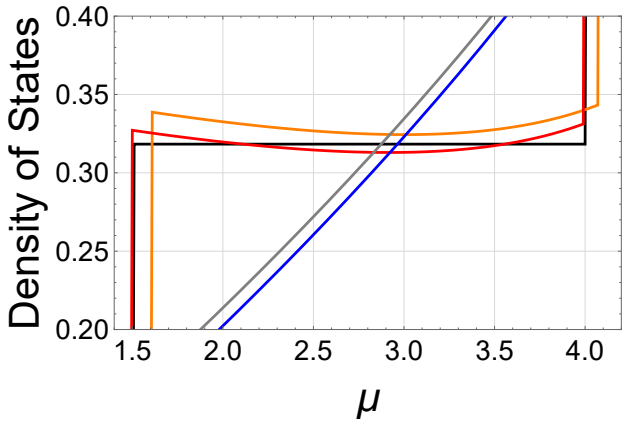

FIG. S5. A zoomed in view of Fig. S4.

Figure S4 shows the density of states of a particular PT slab. This is just the derivative of the number staircase given in Eq. (1) of the main text and shown in Fig. S2. Both TF and GEA2 yield smooth approximations to it, and miss the discrete steps (the origin of the infamous DFT derivative discontinuity [54]). Unlike how it is treated in many semiclassical works [29], the smooth curve is not synonymous with the TF contribution, as GEA2 makes a small but finite correction. The asymptotic expansion approximation contains approximate steps, with approximations to the plateau in between. The exact DOS jumps discontinuously when $\mu = \epsilon_j$ where the ϵ_j are the exact 1D eigenvalues. Using the definition of the saw-tooth function $\langle x \rangle = x - \lfloor x + 1/2 \rfloor$ we can show that the AEA2' approximation jumps when

$$s^{(0)}(\mu) = j + \frac{1}{2}, \qquad j = 0, 1, 2, \cdots . \tag{A1}$$

This is just the lowest order WKB quantization rule for a single 1D well [55]. This means that AEA2' jumps when $\mu = \epsilon_j^{(0)}$, the jth WKB eigenvalue. Similar analysis shows that AEA2 jumps when

$$s^{(2)}(\mu) = j + \frac{1}{2}, \qquad j = 0, 1, 2, \cdots , \tag{A2}$$

which is just the second order WKB quantization rule from Eq. (2) of the main text. Thus AEA2 jumps when $\mu = \epsilon_j^{(2)}$, the second order WKB eigenvalue. AEA2 is much more accurate, as Fig. S5 shows, because $\epsilon_j^{(2)}$ is a better approximation to ϵ_j than $\epsilon_j^{(0)}$. The inaccuracies in both second order AEAs vanish as μ becomes large. Neither curve is quite flat, but AEA2 is flatter than AEA2'.

Appendix B: Densities and potentials

This section contains PT slab densities and PT dimer potentials. Figure S6 shows exact densities, from Table I of

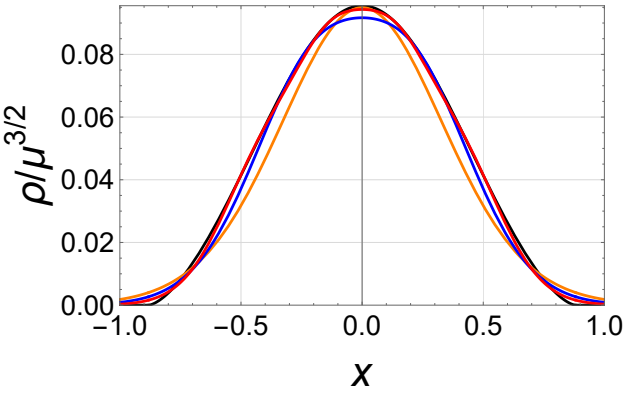

FIG. S6. Densities for $M = 1$ (orange), 2 (blue), 4 (red), and their TF limiting value (black). The areas under the curves are TF (0.0879), M = 1 (0.0809), M = 2 (0.0854), M = 4 (0.0871).

the main text, and their TF approximation–we scaled the densities so that the TF density is the same for all values of M. As M increases we approach the semiclassical limit and these densities weakly approach their TF counterpart. Because the chemical potential (relative to well-depth) is held fixed but the particle number is not (unlike in Fig. 2 of Ref. [44]), the normalization changes, but approaches that of TF in the limit.

Figure S7 simply shows the differences from the TF curve in Fig. S6, making the weak approach to zero evident. Here, weak means that the integral over any well-behaved function times the density approaches its TF counterpart [56].

Figure S8 shows the various potentials of the PT dimer slabs as a function of their separation, given in units of the critical separation at which the second derivative of the midpoint potential vanishes. Beyond this critical value, there are two wells, and the form of the semiclassical asymptotic expansion presented in this work fails.

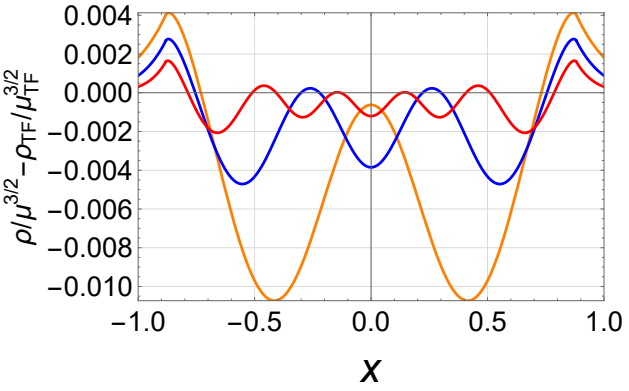

FIG. S7. The deviation of the exact scaled densities in Fig. S6 from the scaled TF density. The exact chemical potential is μ and $\mu_{\rm TF}$ is its TF approximation.

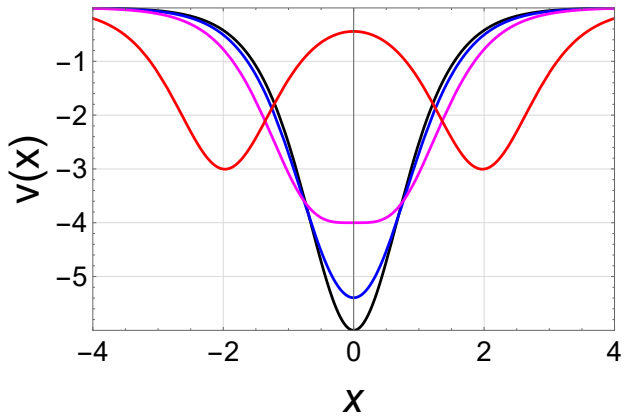

FIG. S8. Several PT dimer potentials made from 2, $D = 3$, PT slabs at various separations: $R/R_c = 0$, 0.5, 1, 3 (black, blue, magenta, red), $R_c = 2\,\mathrm{asech}\sqrt{2/3} = 1.31696$.

Appendix C: Expansion of the 1D action and the derivation and numerical calculation of AEA approximations

The number staircase for the 1D potential $v(x)$ is

$$n(\mu) = \sum_{j=0}^{\infty} \Theta(\mu - \epsilon_j), \tag{C1}$$

where $\Theta(x)$ is the Heaviside step function. It counts the number of occupied levels in a 1D well for a given μ. It can also be written as [24]

$$n(\mu) = s(\mu) - \langle s(\mu) \rangle\,. \tag{C2}$$

This form is more useful for deriving semiclassical approximations to $n(\mu)$ order by order. To derive such approximations we need to expand $s(\mu)$. To fourth order the expansion of the action is [37]

$$\begin{aligned} s^{(0)}(\mu) &= \int dx\, \frac{p_{\rm F}(x)}{\pi}, \qquad \Delta s^{(2)}(\mu) = -\frac{I''(\mu)}{3}, \\ \Delta s^{(4)}(\mu) &= \frac{J'''(\mu)}{5760}, \end{aligned} \tag{C3}$$

where I is in the main text and

$$J = \int dx \frac{7v''(x)^2 - 5v^{(4)}(x)p_{\rm F}(x)^2}{\pi\, p_{\rm F}(x)}, \tag{C4}$$

where again all integration is between the two classical turning points and $v^{(n)}(x)$ is the n-th derivative of $v(x)$.

We define two M-th order 1D number staircase expansions

$$\begin{aligned} n^{(M')}(\mu) &= s^{(M)}(\mu) - \left\langle s^{(M-2)}(\mu) \right\rangle, \\ n^{(M)}(\mu) &= s^{(M)}(\mu) - \left\langle s^{(M)}(\mu) \right\rangle, \end{aligned} \tag{C5}$$

and $n^{(0')}(\mu) = s^{(0)}(\mu)$.

The slab particle number is related to the 1D number staircase via

$$N(\mu) = \int_0^{\mu} d\epsilon\, \frac{n(\epsilon)}{\pi}. \tag{C6}$$

Plugging in $n^{(2)}$ ($n^{(2')}$) and collecting the second order terms yields the AEA2(2') approximation to N.

In this paper we calculate $N^{\rm AEA4'}(\mu)$, the AEA4' approximation to $N(\mu)$, numerically. We start by plugging $n^{(4')}$ into Eq.(C6) to derive

$$\pi N^{\rm AEA4'} = \int_0^{\mu} d\epsilon\, \Delta s^{(4)}(\epsilon) + \int_0^{\mu} d\epsilon\, n^{(2)}(\epsilon). \tag{C7}$$

The integral over $n^{(2)}$ is easy to evaluate numerically because $n^{(2)}(\epsilon)$ always equals an integer. To evaluate the integral over $n^{(2)}(\epsilon)$ we need the ϵ values where $n^{(2)}(\epsilon)$ jumps discontinuously between integer values. From the definition of the saw-tooth function $\langle x \rangle$ in the main text and Eq. (C5), we find that it jumps when

$$s^{(2)}(\epsilon_j) = j + \frac{1}{2}, \qquad j = 0, 1, 2, \cdots. \tag{C8}$$

This is just the second order eigenvalue expansion from Eq. (2) of the main text. More commonly this is called the second order WKB series quantization rule [37]. Inverting this equation numerically yields $\epsilon_j^{(2)}$, the second order WKB series approximation to ϵ_j. The other integral in Eq. (C7) is

$$\int_0^{\mu} d\epsilon\, \Delta s^{(4)}(\epsilon) = \frac{J''(\mu) - J''(0)}{5760}. \tag{C9}$$

To evaluate $J''(0)$ we carefully take the limit of $J''(\mu)$ as $\mu \to 0$ to derive

$$J''(0) = \frac{821 v^{(4)}(0)^2 - 344 v''(0) v^{(6)}(0)}{384 v''(0)^{5/2}}. \tag{C10}$$

We calculate $\mu^{\rm AEA4'}(N)$ by inverting $N^{\rm AEA4'}(\mu)$ numerically. The expression above diverges as $v''(0) \to 0$. This would happen for the pure quartic oscillator, $v(x) = x^4/2$. If it diverges we just set $J''(0)$ to 0.

The exact slab energy is completely specified by the 1D number staircase via Eq. (C6) and

$$E(\mu) = \mu N(\mu) - \int_0^\mu d\epsilon\, N(\epsilon). \tag{C11}$$

Plugging in $n^{(2)}$ ($n^{(2')}$) and collecting second order terms yields $E^{\rm AEA2(2')}(\mu)$. Plugging in $n^{(4')}$ yields

$$E^{\rm AEA4'}(\mu) = E^{\rm AEA2}(\mu) + \frac{\mu J''(\mu) - J'(\mu) + J'(0)}{5760\pi}, \tag{C12}$$

where

$$E^{\rm AEA2}(\mu) = \mu N^{\rm AEA2}(\mu) - \int_0^\mu d\epsilon\, N^{\rm AEA2}(\epsilon), \tag{C13}$$

where

$$N^{\rm AEA2}(\mu) = \int_0^\mu d\epsilon\, \frac{n^{(2)}(\epsilon)}{\pi}. \tag{C14}$$

To compute $E^{\rm AEA2}(\mu)$ numerically we only need the second order WKB series eigenvalues. In the limit $\mu \to 0$ we derive

$$J'(0) = \frac{9v^{(4)}(0)}{8\sqrt{v''(0)}}. \tag{C15}$$

If $v''(0) = 0$ we just set $J'(0)$ to 0. We set the particle number by plugging $\mu^{\rm AEA4'}(N)$ into $E^{\rm AEA4'}(\mu)$: $E^{\rm AEA4'}(N) = E^{\rm AEA4'}[\mu^{\rm AEA4'}(N)]$.

We approximated the AEA4' kinetic energy in Table I, of the main text, by subtracting away the AEA4' potential energy from the AEA4' total energy. The slab potential energy is related to the 1D potential energy via

$$V(\mu) = \int_0^\mu d\epsilon\, \frac{V_{\rm 1D}(\epsilon)}{\pi}. \tag{C16}$$

To evaluate $V^{\rm AEA4'}(\mu)$ numerically we plugged

$$V_{\rm 1D}^{\rm AEA4'}(\mu) = V^{\rm TF}[n^{(4')}(\mu)] + \Delta V^{(2)}[n^{(2')}(\mu)] + \Delta V^{(4)}[n^{(0')}(\mu)], \tag{C17}$$

into the integral above. $V^{\rm TF}(n)$, $\Delta V^{(2)}(n)$, and $\Delta V^{(4)}(n)$ are the lowest, second, and fourth order terms in the LS expansion of the 1D potential energy as a function of the exact 1D particle number, n. For the PT slab these terms are

$$V^{\rm TF}(n) = \sqrt{\frac{D}{2}}\frac{n^2}{2}, \qquad \Delta V^{(2)}(n) = -\frac{n^2}{32\sqrt{2D}},$$
$$\Delta V^{(4)}(n) = \frac{3n^2}{1024\sqrt{2D^3}}, \tag{C18}$$

Everywhere except Table I we approximated the AEA4' kinetic energy by subtracting the exact potential energy from the AEA4' total energy.

Appendix D: Differences between electron removal energies and chemical potentials

This section is devoted to showing how oscillating contributions can give rise to wildly differing accuracies of estimates for electron removal energies, depending on if the total energy curve or the chemical potential is used.

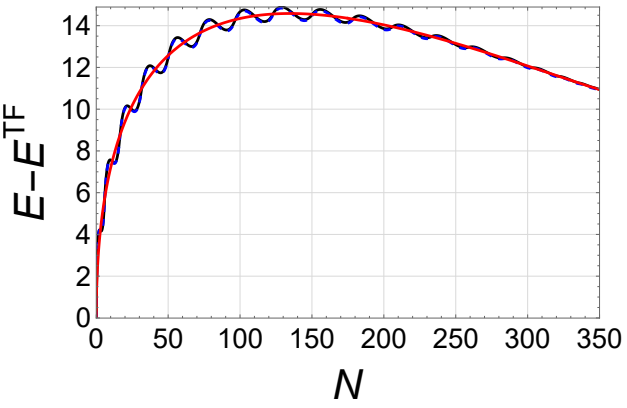

FIG. S9. The exact energy (black) and its AEA2 (red) and AEA4' (blue) approximations (with the TF energy subtracted), for the $M = 5$ PT slab in Table I of the main text.

Figure S9 shows the exact and several approximate energy curves, each with the TF curve subtracted, as a function of N. The black curve (exact) is oscillating, as is the blue (AEA4') approximation. But the red curve (AEA2) contains no oscillations, as the oscillations cancel out of the total energy curve to 2nd order [which means that $E^{\rm AEA2}(\mu) = E^{\rm AEA2'}(\mu)$].

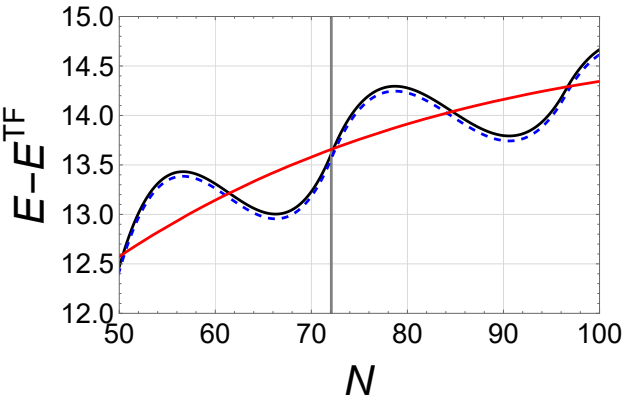

FIG. S10. A zoomed in view of Fig. S9. The gray line marks the occupation we examined in Table I of the main text.

Figure S10 simply zooms in on the energy curve in the region of the particle number corresponding to $\mu = D/2$, marked by the vertical line. Clearly the oscillations play a large role in the energy change if you remove 1/2 an electron when $\mu = D/2$. The red curve yields a very poor approximation to this energy difference. The exact energy

satisfies $E'(N) = \mu$, but $dE^{\rm AEA2}/dN$ yields a poor approximation to the chemical potential. Instead we derive $\mu^{\rm AEA2}(N)$ by inverting $N^{\rm AEA2}(\mu)$. The blue AEA4' curve will clearly yield almost exact answers.

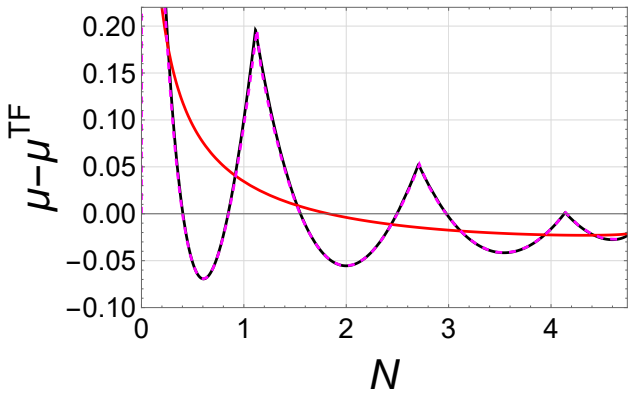

FIG. S11. The exact chemical potential for a PT slab with $D = 10$ (black), $dE^{\rm AEA2}/dN$ (red), and $\mu^{\rm AEA2}(N)$ (magenta). We have subtracted the TF chemical potential from all curves.

Table S1 contains many different approximations, for total energy differences and chemical potentials. Figure S11 shows the exact chemical potential and two approximations to it. The AEA2 chemical potential, calculated by inverting $N^{\rm AEA2}(\mu)$, captures the derivative discontinuities, while $dE^{\rm AEA2}/dN$, does not. This shows that relationships which hold exactly, for TF theory, and for GEA2, namely $E'(N) = \mu$, may fail at any given order when oscillatory terms are involved.

Appendix E: Breakdown of the AEA4' approximation in our bond stretching table

Figure S12 plots several of the errors listed in Table III of the main text as functions of the separation between the PT centers.

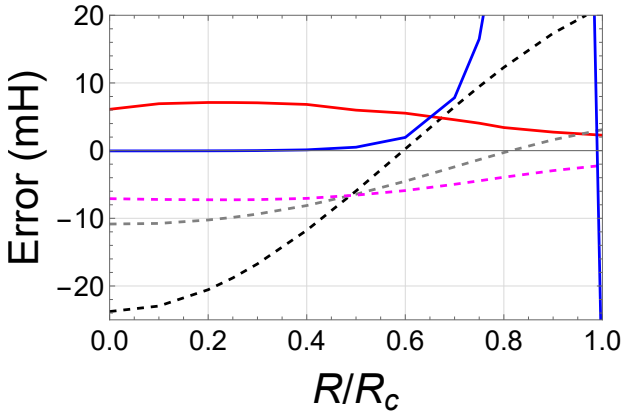

FIG. S12. The errors in Table III of the main text. Legend: TF (black), GEA2 (gray), MGE2 (magenta), AEA2 (red), AEA4' (blue). Functionals acting on the exact density are denoted with dashed lines.

Appendix F: Tables of energies for PT slabs and PT dimers

This section contains tables that supplement those in the main text.

Table S2 shows the total energies (not just the kinetic energies) of the calculations in Table I of the main text. In this case, any functionals evaluated on the exact density include the exact potential energy by construction. Just as in the self-consistent TF calculation, we expect errors on (some version of) self-consistent densities to be larger.

Tables S3-S5 supplement Table III of the main text, showing total kinetic energies of the PT dimer slabs, not just binding energies, so that approximations cannot benefit from cancellation of errors between the PT dimer slab and the separated 'atomic' slabs. We also give the corresponding total energy and binding energy.

Table S6 shows the 1D ground state WKB eigenvalues and their leading corrections for the PT dimer as a function of well-separation. By $R = 0.8R_c$, the leading correction has a larger error than WKB itself, signaling the incipient failure of the asymptotic series.

			Errors (mH)						
			IP			μ			
M	IP	μ	TF	AEA2	AEA4'	TF	AEA2'	AEA2	AEA4'
1	5.557	6.342	−63	−3	0.0622	−242	−41	0.010	−0.0532
2	17.607	18.000	−172	−131	0.0168	−239	−21	0.013	−0.0126
3	35.224	35.486	−204	−166	0.0061	−238	−14	0.009	−0.0048
4	58.603	58.799	−217	−180	0.0028	−237	−11	0.006	−0.0023
5	87.784	87.941	−224	−187	0.0015	−237	−9	0.004	−0.0013
6	122.781	122.912	−227	−191	0.0009	−237	−7	0.003	−0.0008
7	163.599	163.711	−230	−194	0.0006	−237	−6	0.003	−0.0005
8	210.240	210.339	−231	−196	0.0004	−237	−5	0.002	−0.0004
9	262.707	262.794	−232	−197	0.0003	−237	−5	0.002	−0.0003
10	321.000	321.079	−233	−198	0.0002	−237	−4	0.001	−0.0002

TABLE S1. Same as Table II of the main text but with the AEA2' and AEA4' approximations.

				Errors (mH)						
				Potential Functionals			Density Functionals			
M	D	N	E/N	TF	AEA2	AEA4'	TF	GEA2	MGE2	GEA4
1	12.685	1.293	4.312	−192	9.2	0.02522	−156	−41	−8	−2
2	36.000	6.525	12.189	−190	3.1	0.00298	−159	−35	1	−6
3	70.971	18.318	24.005	−189	1.6	0.00076	−162	−31	7	−7
4	117.599	39.293	39.759	−189	0.9	0.00027	−164	−28	11	−6
5	175.883	72.075	59.451	−189	0.6	0.00012	−165	−26	14	−6
6	245.824	119.288	83.082	−189	0.4	0.00006	−166	−25	16	−6
7	327.422	183.555	110.651	−189	0.3	0.00004	−167	−24	18	−6
8	420.677	267.500	142.159	−189	0.3	0.00002	−168	−23	19	−6
9	525.589	373.746	177.605	−189	0.2	0.00001	−168	−22	21	−5
10	642.157	504.918	216.990	−189	0.2	0.00001	−169	−21	22	−5

TABLE S2. Same as Table I of the main text, but for the total energy.

		Errors (mH)									
		Potential Functionals					Exact Density or μ				
R/R_c	T	TF	GEA2	AEA2'	AEA2	AEA4'	TF	GEA2	MGE2	GEA4	AEA4'(μ)
0	1.890	34	−19	11.84	3.1	0.02	−77	−22	−5.5	−12	0.20
0.1	1.881	36	−16	12.51	3.9	0.02	−76	−21	−5.6	−12	0.20
0.2	1.858	39	−12	12.24	4.1	0.04	−74	−21	−5.6	−12	0.19
0.25	1.840	40	−9	11.90	4.1	0.05	−72	−21	−5.6	−12	0.19
0.3	1.820	42	−6	11.48	4.0	0.07	−70	−20	−5.6	−12	0.18
0.4	1.770	46	1	10.31	3.8	0.18	−65	−19	−5.4	−11	0.18
0.5	1.711	49	8	8.39	2.9	0.57	−59	−17	−5.0	−10	0.21
0.6	1.644	50	14	6.74	2.5	2.01	−53	−15	−4.3	−9	0.35
0.7	1.575	50	17	4.49	1.5	7.89	−47	−13	−3.4	−7	0.71
0.75	1.539	49	18	3.32	1.0	16.56	−44	−12	−2.8	−7	1.00
0.8	1.504	47	17	2.00	0.4	37.29	−41	−11	−2.3	−6	1.38
0.9	1.435	43	16	−0.02	−0.3	315.89	−36	−9	−1.3	−4	2.43
1	1.369	37	12	−1.79	−0.8	−37.27	−32	−8	−0.6	−3	−0.26

TABLE S3. Same as Table III of the main text, but showing the total kinetic energies, not the kinetic binding energies.

		Errors (mH)							
		Potential Functionals			Exact Density or μ				
R/R_c	$E-2E_A$	TF	AEA2	AEA4'	TF	GEA2	MGE2	GEA4	AEA4'(μ)
0	1.174	−39	−9.2	−0.04	−23.8	−10.8	−7.1	−12	−0.23
0.1	1.162	−39	−9.4	−0.04	−23.0	−10.8	−7.2	−12	−0.24
0.2	1.127	−36	−9.7	−0.03	−20.5	−10.2	−7.3	−12	−0.24
0.25	1.100	−34	−9.9	−0.02	−18.8	−9.9	−7.3	−12	−0.25
0.3	1.068	−32	−10.0	0.01	−16.7	−9.4	−7.2	−12	−0.25
0.4	0.988	−27	−10.1	0.12	−11.8	−8.1	−7.1	−12	−0.25
0.5	0.887	−21	−9.7	0.51	−6.0	−6.4	−6.6	−11	−0.22
0.6	0.767	−13	−8.7	1.95	0.3	−4.5	−5.9	−9	−0.08
0.7	0.630	−6	−7.2	7.82	6.5	−2.4	−5.0	−8	0.27
0.75	0.556	−2	−6.3	16.49	9.5	−1.3	−4.5	−7	0.57
0.8	0.479	2	−5.3	37.23	12.3	−0.3	−3.9	−6	0.95
0.9	0.315	9	−3.4	315.82	17.3	1.6	−3.0	−4	2.00
1	0.143	15	−1.7	−37.33	21.3	3.1	−2.2	−3	−0.69

TABLE S4. Same as Table III of the main text, but with the total binding energy.

		Errors (mH)							
		Potential Functionals			Exact Density or μ				
R/R_c	E	TF	AEA2	AEA4'	TF	GEA2	MGE2	GEA4	AEA4'(μ)
0	2.845	−99	−7.0	0.02	−77	−22	−5.48	−12	0.20
0.1	2.833	−98	−7.1	0.02	−76	−21	−5.60	−12	0.20
0.2	2.798	−95	−7.4	0.04	−74	−21	−5.64	−12	0.19
0.25	2.772	−94	−7.6	0.05	−72	−21	−5.65	−12	0.19
0.3	2.740	−92	−7.7	0.07	−70	−20	−5.62	−12	0.18
0.4	2.659	−86	−7.8	0.18	−65	−19	−5.44	−11	0.18
0.5	2.558	−80	−7.4	0.57	−59	−17	−4.96	−10	0.21
0.6	2.438	−73	−6.5	2.01	−53	−15	−4.29	−9	0.35
0.7	2.301	−65	−5.0	7.89	−47	−13	−3.36	−7	0.71
0.75	2.227	−61	−4.0	16.56	−44	−12	−2.84	−7	1.00
0.8	2.150	−57	−3.1	37.29	−41	−11	−2.31	−6	1.38
0.9	1.986	−51	−1.2	315.89	−36	−9	−1.33	−4	2.43
1	1.814	−45	0.5	−37.27	−32	−8	−0.56	−3	−0.26

TABLE S5. Same as Table III of the main text, but with the total energy relative to the bottom of the well. The dimer well depth is $\mathcal{D} = 6\,\mathrm{sech}^2(R/2)$.

		Errors	
R/R_c	ϵ_0	WKB0	WKB2
0	1.500	0.107	−0.00056
0.1	1.489	0.106	−0.00061
0.2	1.456	0.101	−0.00078
0.25	1.431	0.097	−0.00094
0.3	1.402	0.093	−0.00116
0.4	1.329	0.083	−0.00194
0.5	1.239	0.069	−0.00347
0.6	1.134	0.053	−0.00640
0.7	1.016	0.034	−0.01186
0.75	0.954	0.024	−0.01604
0.8	0.890	0.013	−0.02153
0.9	0.756	−0.011	−0.03734
1	0.618	−0.036	−0.06000
∞	2.000	0.199	−0.00208

TABLE S6. The exact ground state eigenvalues (relative to the bottom of the well) and their zeroth and second order WKB approximations for the PT dimers in Table III of the main text. The last row, $R/R_c = \infty$, corresponds to 2, $D = 3$, PT slabs infinity far apart (so all of the quantities are double those of a single PT slab).